Online ISSN: 2981-0396 Print ISSN: 2981-0388

International Journal of Iron & Steel Society of Iran

Journal Homepage: https://journal.issiran.com/

Research Article

Structure and Magnetic Properties of $(Mg_{0.2}Ti_{0.2}Zn_{0.2}Cu_{0.2}Fe_{0.2})_3O_4$ High Entropy Oxides Synthesized by Different Iron Oxides

T. Isfahani *[1]

Materials Engineering Group, Golpayegan College of Engineering, Isfahan University of Technology, Golpayegan, Iran

ARTICLE INFO

Keywords:

$(Mg_{0.2}Ti_{0.2}Zn_{0.2}Cu_{0.2}Fe_{0.2})_3O_4$ High Entropy Oxide, Fe_2O_3, Fe_3O_4, Structure, Magnetic Property.

Article history:

Received 18 March 2025
Received in revised form 31 May 2025
Accepted 19 August 2025

ABSTRACT

The introduction of high-entropy material has provided the possibility of efficiently producing low-cost advanced materials with several unique properties suitable for industries. High-entropy materials have gained significant interest because they can be tailored to have functional properties. Among the high-entropy material are the high entropy oxides. The objective of this study was to synthesize $(Mg_{0.2}Ti_{0.2}Zn_{0.2}Cu_{0.2}Fe_{0.2})_3O_4$ high entropy oxides (HEO) using different iron sources of Fe_2O_3, Fe_3O_4, and Fe_2O_3/Fe_3O_4 mixture and to study their structure and magnetic properties. Solid state synthesis method was used to obtain $(Mg_{0.2}Ti_{0.2}Zn_{0.2}Cu_{0.2}Fe_{0.2})_3O_4$ using low-cost raw materials and different iron sources. The XRD diffraction patterns along with the Rietveld analysis indicated that for the three iron source(s), a pure single-phase $Fd\bar{3}m$ spinel structure was obtained after the heat treatment at 1000 ℃ for 24 hours. The SEM images and elemental MAP analysis indicated that the powders were agglomerated with semi-spherical morphology and the constituent elements were uniformly distributed. Magnetic test results obtained from the VSM test revealed that the magnetic properties are severely influenced by the iron source used for the synthesis of the $(Mg_{0.2}Ti_{0.2}Zn_{0.2}Cu_{0.2}Fe_{0.2})_3O_4$ HEO samples. The HEO samples obtained using the Fe_3O_4 sample had better magnetic properties (Ms= 13.93, Mr= 4.39, and Hc=350) compared to the other two samples.

1. Introduction

Recently, attention has been given to the request of industries to replace traditional ceramics (iron oxide, magnesium oxide, aluminum oxide, zirconia oxide, titanium oxide, copper oxide, zinc oxide, etc.) with low cost and high performance advanced ceramics. High-entropy oxides have made the contradiction of having advanced properties at a low price possible. Rost et al were the first to introduce the "entropy stabilized oxides". The chemically complex oxides named as high-entropy oxides (HEOs) are single-phase oxides that incorporate five different cations in equi-atomic ratios [1-4]. The multi-cationic equi-atomic HEOs are located at the centers of multinary phase diagrams [5-7]. Several researchers have shown that the HEOs have unexpected, fascinating, and advanced behaviors [8, 9]. As mentioned, the HEOs are entropy-stabilized oxides with a single-phase crystal structure. HEOs are obtained by increasing

* *Corresponding Author*
Email: t.isfahani@iut.ac.ir
Address: Materials Engineering Group, Golpayegan College of Engineering, Isfahan University of Technology, Golpayegan, Iran
1. Assistant Professor

DOI: http://10.22034/IJISSI.2025.2056169.1320
Published by ISSI (Iron & Steel Society of Iran)

the configurational entropy (S_{config}) of the system. Increased S_{config} of the system is obtained by increasing the number of elements that are randomly located at the same lattice sites. Molar configurational entropy of oxide systems can be obtained by Eq.(1) [1, 8]. Mole fraction of elements in the anion and cation sites are x_j and x_i, respectively. R is the universal gas constant. Murthy et al [1, 8] classified materials as high, medium, and low entropy materials where they have $S_{config} \geq 1.5R$, $1.5R > S_{config} > 1R$, and $S_{config} < 1R$; respectively. From Eq.(1) it can be revealed that an equiatomic five- cation system has a S_{config} of 1.61 R.

$$S_{config} = -R\left[\left(\sum_{i=1}^{N} x_i Ln x_i\right)_{cation\ site} + \left(\sum_{j=1}^{M} x_j Ln x_j\right)_{anion\ site}\right] \quad \text{Eq.(1)}$$

In most cases, when the system has a $S_{config} \geq 1.5R$, a single-phase is obtained. It has also been shown that this criterion is not a guarantee, and there are exceptions. Precisely, it can be mentioned that a single phase is only obtained when the $T\Delta S_{mix}$ is large enough to dominate the free energy and prevail over the ΔH_{mix} (according to Eq.(2)). Otherwise, intermediate phases are obtained with higher formation enthalpies[9].

$$\Delta G_{mix} = \Delta H_{mix} - T\Delta S_{mix} \quad \text{Eq.(2)}$$

Up to now, several HEOs such as $(Co_{0.2}Cu_{0.2}Mg_{0.2}Ni_{0.2}Zn_{0.2})O$ and $(Mg_{0.2}Ti_{0.2}Zn_{0.2}Cu_{0.2}Fe_{0.2})_3O_4$ [2, 10] have been introduced, mainly having low cost and enhanced properties compared to their counterparts. The HEO has several unique properties, such as thermal stability, resistance to corrosion or oxidation, and wear resistance. Due to the importance of HEO and their rapid development, more detailed information is necessary. In this research, the $(Mg_{0.2}Ti_{0.2}Zn_{0.2}Cu_{0.2}Fe_{0.2})_3O_4$ HEO powders were synthesized (using different iron oxide sources of Fe_2O_3, Fe_3O_4, and their mixture), and their effect on the structure and magnetic properties was studied.

2. Materials and Methods

2.1. Synthesis of $(Mg_{0.2}Ti_{0.2}Zn_{0.2}Cu_{0.2}Fe_{0.2})_3O_4$ HEO

The $(Mg_{0.2}Ti_{0.2}Zn_{0.2}Cu_{0.2}Fe_{0.2})_3O_4$ HEO powders were prepared using the solid-state method. MgO, TiO_2, ZnO, CuO, FeO, Fe_2O_3, and Fe_3O_4 powders of analytical purity (>99.9 %) were used as starting material without any further purification. The slight oxygen deficit in high entropy oxides is overcome during long heat treatment times in air, resulting in the oxidation or by forming vacancies (non-stoichiometric). Equimolar amounts of the oxides were milled for 5 hours using a high-energy planetary ball mill using zirconia balls according to Table 1. Milled powders were heat-treated at 1000°C for 24 hours. Rietveld analysis was applied to the XRD patterns using Topas software to obtain detailed information on the purity and the formed structure.

2.2. Materials Characterization

The phase purity and structure were characterized by a Phillips X-ray diffraction machine (XRD). XRD patterns were obtained using 40 kV and 30 mA under Cu-Kα radiation. XRD pattern was collected at 2Θ= 20-90° using a scan speed of 1°/min. Rietveld refinement phase analysis was done using Topas software. SEM (TESCAN-Mira 3) and MAP analysis were used to obtain information on the particle morphology, size, and elemental distribution. The VSM machine was used to get information on the magnetic properties from the hysteresis loops obtained at room temperature.

3. Results and Discussion

3.1. XRD Analysis

XRD patterns of the starting powder mixtures, 5 hour milled powder mixtures, and 24-hour heat treated milled powders at 1000°C are presented in Fig. 1(a)-(i). for the HEO-2, HEO-3, and HEO-23 samples, respectively. For the synthesis of $(Mg_{0.2}Ti_{0.2}Zn_{0.2}Cu_{0.2}Fe_{0.2})_3O_4$ HEO powders, the starting powders of MgO, TiO_2, ZnO, and CuO, along with different iron oxide sources of Fe_2O_3 (Fig. 1(a).), Fe_3O_4 (Fig. 1(c).), and a mixture of Fe_3O_4

Table 1. Sample code and the initial material used for the synthesis of the $(Mg_{0.2}Ti_{0.2}Zn_{0.2}Cu_{0.2}Fe_{0.2})_3O_4$ HEO powders.

Sample code	The initial powder used for the synthesis
HEO-2	MgO, TiO_2, ZnO, CuO, FeO, and Fe_2O_3
HEO-3	MgO, TiO_2, ZnO, CuO, FeO, and Fe_3O_4
HEO-23	MgO, TiO_2, ZnO, CuO, FeO, Fe_2O_3, and Fe_3O_4

and Fe_2O_3 (Fig. 1(b).) were used. As can be seen from the XRD patterns presented in Fig. 1(a)-(c)., there is no indication of impurities in the starting powders. This result indicates that the starting powders have high purity and are free from contamination. The powder mixtures milled for 5 hours (Fig. 1 (d)-(e).) showed that the powders are low in crystallinity. The low crystallinity of the XRD pattern is due to the reduced crystallite size and increased strain. The reduced crystallite size and increased strain is induced to the powder mixture during the milling process and also because no reaction has occurred during the milling process. According to Fig. 1(g)-(i)., it can also be seen that heat treatment at 1000°C for 24 hours is sufficient for the solid-state reaction to occur. Solid state reaction results in a pure single-phase for all the samples (HEO-2, HEO-3, and HEO-23). It can be seen from the XRD patterns that, despite the use of different iron oxide sources, all the patterns are identical and have the same $Fd\bar{3}m$ spinel crystal structure. The obtained single-phase HEO also indicates that the oxygen deficit calculated to be received by the combination of oxides used as the starting material has been overcome by the long heat treatment in air. Diffraction peaks at two thetas of 29.89, 35.26, 36.95, 42.79, 53.25, 56.64, 62.18, 73.56, and 89.09 are related to planes of (111), (220), (311), (222), (400), (422), (511), (440), (533), and (731), respectively.

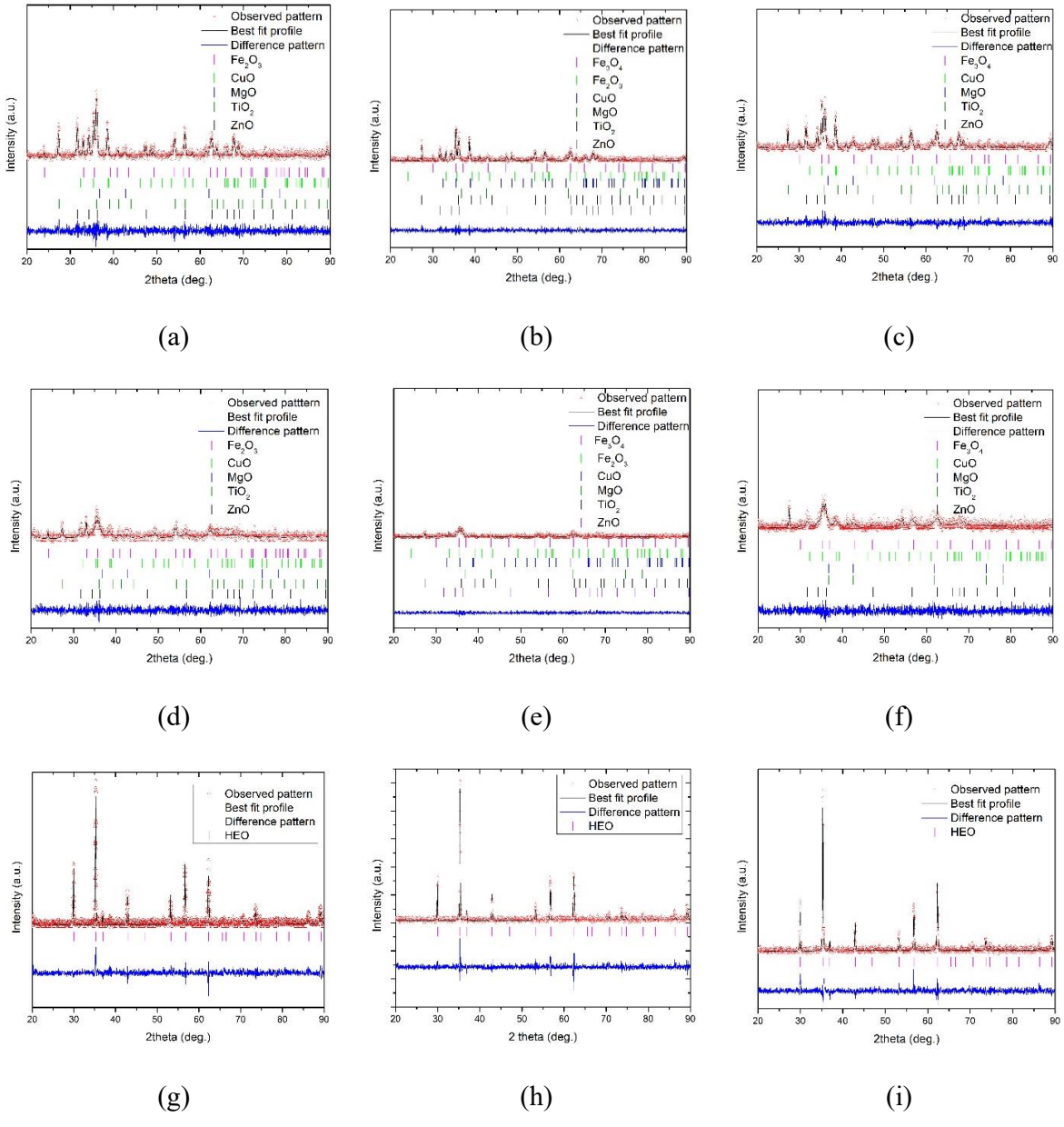

Fig. 1. The XRD patterns and Rietveld analysis of the starting powder mixtures (a-c), 5 hour milled powder mixtures (d-f), and 24-hour heat treated milled powders at 1000°C (g-i) are presented for the HEO-2 (a, d, and g), HEO-3 (c, f, and i), and HEO-23 (b, e, and h) samples.

3.2. SEM Analysis

Fig. 2. shows the SEM image of the synthesized $(Mg_{0.2}Ti_{0.2}Zn_{0.2}Cu_{0.2}Fe_{0.2})_3O_4$ HEO particles (Fig. 2(a).) along with EDS elemental mapping of the Mg, Ti, Zn, Cu, and Fe elements (Fig. 2 (b).) for the HEO-3 sample. It can be seen from Fig. 2 (a). that the particles have semi-spherical morphology and that the Mg, Ti, Zn, Cu, Fe, and O elements have a homogeneous distribution (Fig. 2(b)). Homogeneous distribution of elements confirms the successful synthesis of the single-phase $(Mg_{0.2}Ti_{0.2}Zn_{0.2}Cu_{0.2}Fe_{0.2})_3O_4$ HEO. The particles form large agglomerates, and the particle sizes are in the range of 34-96 nm with a mean diameter of 49.3 nm.

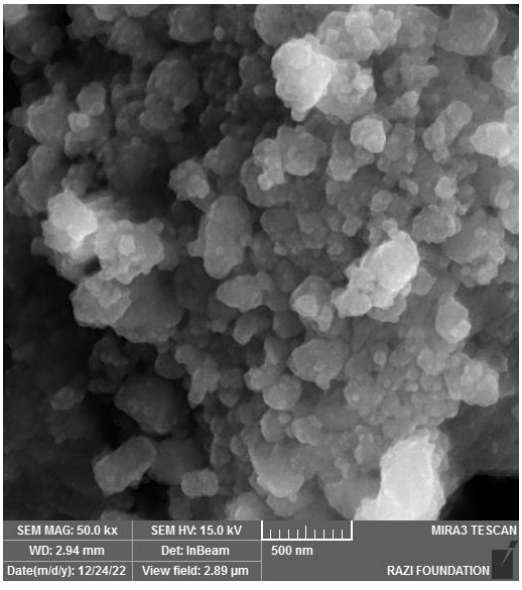

(a)

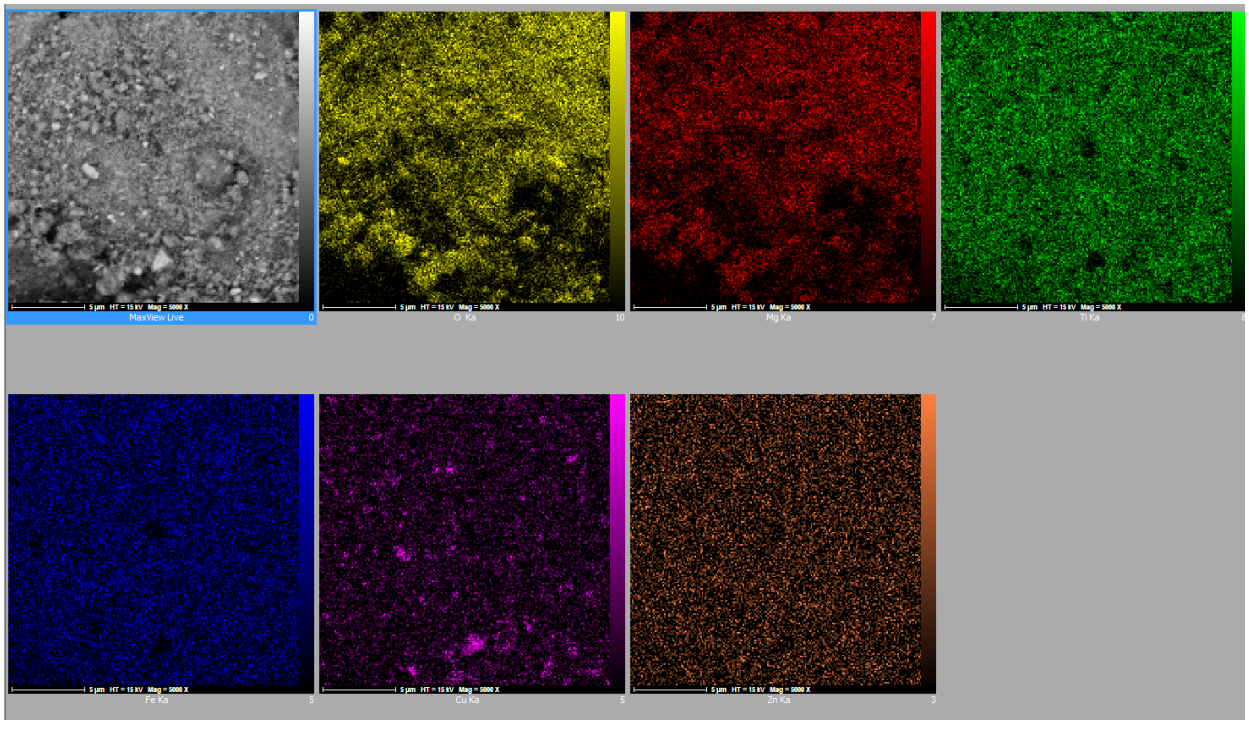

(b)

Fig. 2. The SEM image of the $(Mg_{0.2}Ti_{0.2}Zn_{0.2}Cu_{0.2}Fe_{0.2})_3O_4$ HEO synthesized using Fe_3O_4 (HEO-3) (a) along with the MAP of its constituent elements (b).

3.3. Magnetism Measurement

The magnetic properties of the $(Mg_{0.2}Ti_{0.2}Zn_{0.2}Cu_{0.2}Fe_{0.2})_3O_4$ HEO particles synthesized using different sources of iron oxide are studied using a vibrating sample magnetometer (VSM) test. Magnetic properties are obtained using the hysteresis loops at room temperature with varying magnetic fields. Magnetic properties measured by a Vibrating Sample Magnetometer (VSM) machine are influenced by a variety of intrinsic (material-specific) and extrinsic (experimental) parameters. Intrinsic material parameters include composition, crystal structure (material type, crystal anisotropy, and phase purity), and microstructural factors (grain size, domain structure, and internal stress/strain). In comparison, the extrinsic experimental parameters are sample geometry and preparation (shape anisotropy, mass/volume, and sample mounting), measurement conditions (temperature, Curie/Neel temperature, applied magnetic field, field strength, field direction, and sweep rate), and instrument-specific factors (calibration, vibration settings, noise, detection limits). It should be noted that coercivity (Hc) is influenced by grain size, anisotropy, and defects. Saturation magnetization (Ms) depends on material composition and density. The remanence (Mr) is linked to the domain structure and pinning sites, while the susceptibility is affected by the temperature and sample geometry [11-13]. VSM test plots and the obtained results of the $(Mg_{0.2}Ti_{0.2}Zn_{0.2}Cu_{0.2}Fe_{0.2})_3O_4$ HEO particles obtained using Fe_2O_3, Fe_3O_4, and a mixture of Fe_2O_3 and Fe_3O_4 in the initial material are presented in Fig. 3. and Table 2., respectively. Saturation magnetization (Ms) was 0.31, 13.93, and 10.14 for HEO-2, HEO-3, and HEO-23 samples, respectively. The remanence magnetization (Mr) was 0.04, 4.39, and 3.23, respectively. It is well known that Fe_2O_3 exists in two forms of hematite (α-Fe_2O_3) and maghemite (γ-Fe_2O_3). Hematite is weakly magnetic and irrelevant for hard/soft classification. In contrast, maghemite is ferrimagnetic with moderate coercivity, known as soft (sometimes labeled as semi-hard). Fe_3O_4 is known as magnetite and is a ferrimagnetic material. This means it has a spontaneous magnetization where the magnetic moments are aligned in opposite directions along with unequal magnitude resulting a net magnetic moment. The Fe_3O_4 is considered to be a soft magnet and sometimes as semi-hard. Magnetite has high saturation magnetization like soft magnets although its coercivity is higher than typical soft material. It can also be easily magnetized and demagnetized [14-20]. Therefore, the difference in the magnetic properties of the HEO-2, HEO-3, and HEO-23 samples is acceptable and justifiable.

Hc values of all the samples were in the range of hard magnetic materials (125-12000 Oe), indicating that they can be used as independent magnetic sources. In comparison, the Hc of soft magnetic materials is known to be Hc<100 Oe. The coercivity depends on particle size and structure. Hard magnetic materials with high coercivity resist demagnetization, while soft ones with low coercivity are easily magnetized and demagnetized. Coercivity (Hc) helps determine the type of magnetic material and is the field required to reduce the total magnetization to zero. High coercivity (Hc>10000) indicates that the material is challenging to demagnetize (hard magnetic material). In contrast, low coercivity suggests that the material can be easily demagnetized (soft magnetic material). Soft magnetic material (HC<100) is used in applications where rapid magnetization and demagnetization is needed and hard magnetic materials are used in permanent magnets [21-29].

The magnetic property is characterized by the magnetic hysteresis loops with varying magnetic fields at room temperature. Results showed that using Fe_3O_4 (HEO-3 and HEO-23) increased the intensity of the saturation magnetization (Ms). The Ms was 13.93 $emug^{-1}$ for the HEO-3 sample, while it was 0.31 when Fe_2O_3 (HEO-2) was used. Furthermore, the value of Ms for the HEO-23 sample was 10.14 which is between the amount of the HEO-2 and HEO-3 samples. Moreover, the remanence magnetization (Mr) (4.39 $emug^{-1}$) and the coercive forces (Hc) (350 Oe) were also higher for the HEO-3 sample.

Table 2. Magnetic properties obtained from the hysteresis loop of the VSM test.

Sample	Ms	Mr	Hc
HEO-2	0.31	0.04	134.41
HEO-3	13.93	4.39	350
HEO-23	10.14	3.23	320

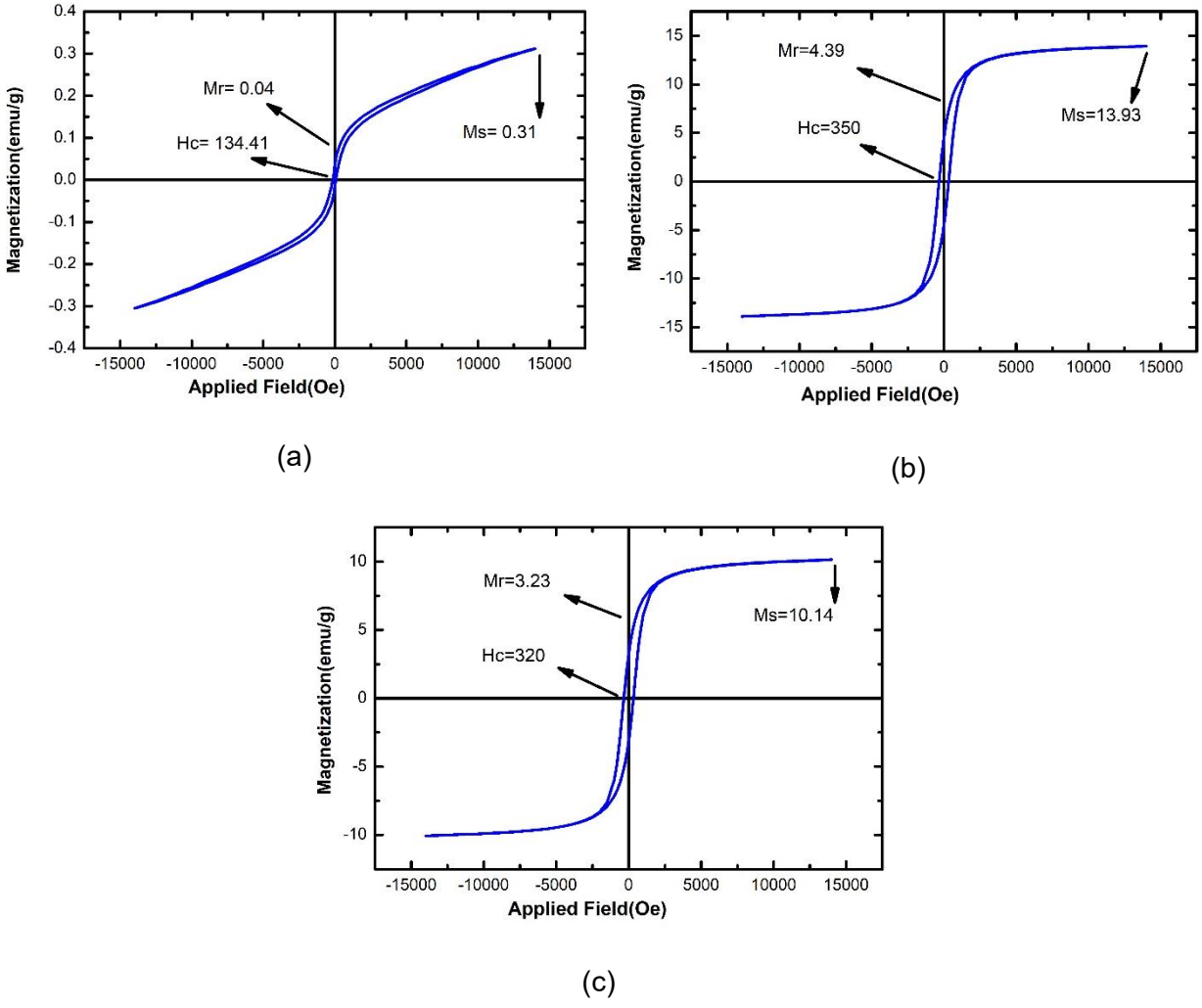

Fig. 3. The hysteresis loops obtained by the VSM test for (a) HEO-2, (b) HEO-3, and (c) HEO-23 samples.

4. Conclusions

In this research, it has been shown that the successful preparation of spinel $(Mg_{0.2}Ti_{0.2}Zn_{0.2}Cu_{0.2}Fe_{0.2})_3O_4$ HEO is possible using different iron sources (Fe_2O_3, Fe_3O_4, and a mixture of them). The $(Mg_{0.2}Ti_{0.2}Zn_{0.2}Cu_{0.2}Fe_{0.2})_3O_4$ HEO powder synthesis was done by a facile one-step solid-state reaction method. The obtained powders synthesized using different iron sources had the same crystal structure of $Fd\bar{3}m$, whereas the magnetic properties were different. The sample synthesized only using Fe_2O_3 as the iron source had the magnetic properties of Ms= 0.31, Mr= 0.04, and Hc= 134.41, while the sample obtained only using Fe_3O_4 as the iron source had the best magnetic properties of Ms= 13.93, Mr= 4.39, and Hc= 350.

References

[1] Sarkar A, et al. High-Entropy Oxides: Fundamental Aspects and Electrochemical Properties, Adv Mater. 2019; 31(26): 1806236.

[2] Rost C.M, et al. Entropy-stabilized oxides, Nat Commun. 2015; 6(1): 8485.

[3] Yeh J.W, et al. Nanostructured High-Entropy Alloys with Multiple Principal Elements: Novel Alloy Design Concepts and Outcomes, Adv Eng Mater. 2004; 6(5): 299-303.

[4] Cantor B, et al. Microstructural development in equiatomic multicomponent alloys, Mater Sci Eng A. 2004; 375-377: 213-218.

[5] Bérardan D, et al. Colossal dielectric constant in high entropy oxides. Phys Status Solidi RRL. 2016; 10(4): 328-333.

[6] Berardan D, et al. Controlled Jahn-Teller distortion in (MgCoNiCuZn)O-based high entropy oxides, J Alloys Compd. 2017; 704: 693-700.

[7] Bérardan D, et al. Room temperature lithium superionic conductivity in high entropy oxides, J Mater Chem A. 2016; 4(24): 9536-9541.

[8] Murty B.S, Yeh J.W, Ranganathan S, High-Entropy Alloys, London: Butterworth-Heinemann. 2014.

[9] Miracle D.B, Senkov O.N, A critical review of high entropy alloys and related concepts, Acta Mater. 2017; 122: 448-511.

[10] Chen H, et al. A new spinel high-entropy oxide $(Mg_{0.2}Ti_{0.2}Zn_{0.2}Cu_{0.2}Fe_{0.2})_3O_4$ with fast reaction kinetics and excellent stability as an anode material for lithium ion batteries, RSC Adv. 2020; 10(16): 9736-9744.
[11] Ge J, et al. Biocompatible Fe_3O_4/chitosan scaffolds with high magnetism, Int J Biol Macromol. 2019; 128: 406-413.
[12] Akhtar M.N, Khan M.A, Effect of rare earth doping on the structural and magnetic features of nanocrystalline spinel ferrites prepared via sol gel route, J Magn Magn Mater. 2018; 460: 268-277.
[13] Gayen A, et al. Effects of composition, thickness and temperature on the magnetic properties of amorphous CoFeB thin films, J Alloys Compd. 2017; 694: 823-832.
[14] Revia R.A, Zhang M, Magnetite nanoparticles for cancer diagnosis, treatment, and treatment monitoring: recent advances, Mater Today. 2016; 19(3): 157-168.
[15] Oroujizad S, Kashi M, Montazer A.H, Fine-tuning magnetic and hyperthermia properties of magnetite (Fe_3O_4) nanoparticles by using ammonia as a reducing agent, Physica B. 2023; 671: 415393.
[16] Marć M, et al. The Use of Ultra-Small Fe_3O_4 Magnetic Nanoparticles for Hydrothermal Synthesis of Fe_3+-Doped Titanate Nanotubes, Materials. 2020; 13(20): 4612.
[17] Nguyen M.D, et al. Fe_3O_4 Nanoparticles: Structures, Synthesis, Magnetic Properties, Surface Functionalization, and Emerging Applications, Appl Sci. 2021; 11(23): 11301.
[18] Avram A, et al. Synthesis and Characterization of γ-Fe_2O_3 Nanoparticles for Applications in Magnetic Hyperthermia. 2011.
[19] Zhang X, et al. Synthesis, optical and magnetic properties of α-Fe_2O_3 nanoparticles with various shapes, Mater Lett. 2013; 99: 111-114.
[20] Can M, Coşkun M, Firat T, A comparative study of nanosized iron oxide particles; Magnetite (Fe_3O_4), maghemite (γ-Fe_2O_3) and hematite (α-Fe_2O_3), using ferromagnetic resonance, J Alloys Compd. 2012; 542: 241-247.
[21] Coey J.M.D, Parkin S.S, History of Magnetism and Basic Concepts. In: Handbook of Magnetism and Magnetic Materials, Cham: Springer. 2021.
[22] Asti G, Recent developments in hard magnetic materials, Hyperfine Interact. 1989; 45(1): 21-33.
[23] Wang W, et al. Low-Loss Soft Magnetic Materials and Their Application in Power Conversion: Progress and Perspective, Energies. 2025; 18(3): 482.
[24] Huber C, et al. Coercivity enhancement of selective laser sintered NdFeB magnets by grain boundary infiltration, Acta Mater. 2019; 172: 66-71.
[25] Herzer G, Grain size dependence of coercivity and permeability in nanocrystalline ferromagnets, IEEE Trans Magn. 1990; 26(5): 1397-1402.
[26] Zhou J, You J, Keqiang Q, Advances in Fe-based amorphous/nanocrystalline alloys, J Appl Phys. 2022; 132: 040702.
[27] Vazquez A, Sotolongo-Costa O, Domain wall dynamics in soft magnetic materials. 1999.
[28] Mörée G, Leijon M, Review of Hysteresis Models for Magnetic Materials, Energies. 2023; 16(9): 3908.
[29] Milyutin V, et al. Machine learning assisted optimization of soft magnetic properties in ternary Fe-Si-Al alloys, J Mater Res Technol. 2024; 29: 5060-5073.